

Oxidization engineered Dzyaloshinskii-Moriya interaction and topological magnetism at Fe/MgO bilayers

Liming Wang,^{1,2} Yonglong Ga,³ Qirui Cui,³ Peng Li,³ Jinghua Liang,³ Yan Zhou^{①,4},
Shouguo Wang,^{1,*} and Hongxin Yang^{②,3,†}

¹Anhui Key Laboratory of Magnetic Functional Materials and Devices, School of Materials Science and Engineering, Anhui University, Hefei 230601, China

²National Laboratory of Solid State Microstructures, School of Physics, Collaborative Innovation Center of Advanced Microstructures, Nanjing University, Nanjing 210093, China

³Ningbo Institute of Materials Technology and Engineering, Chinese Academy of Sciences, Ningbo 315201, China

⁴School of Science and Engineering, The Chinese University of Hong Kong, Shenzhen 518172, China



(Received 25 June 2023; revised 30 October 2023; accepted 12 November 2023; published 5 December 2023)

Fe/MgO system is the one of the most important material prototypes in modern magnetic devices owing to its rich physics such as large perpendicular magnetic anisotropy and magnetoresistance effect. However, both large Dzyaloshinskii-Moriya interaction (DMI) and the topological magnetism that are mostly observed in heavy metals/ferromagnet (oxide) heterostructures have not been reported in this system. Here, we present evidence for sizable DMI that is even comparable to the Co/Pt interface can also be realized at pure and oxidized Fe/MgO bilayers due to the Rashba effect. More importantly, we find that both the strength and chirality of DMI can be engineered via interfacial oxygen manipulation, e.g., oxidization degree. The microscopic mechanism of oxidization inducing $3d$ orbitals reconstruction of Fe atoms dominates the variation of DMI is also unveiled. Using micromagnetic simulations, we further confirm that zero-field chiral spin textures can be achieved at the designed Fe/MgO films. These results not only enrich the physics of Fe/MgO interface but also provide a possible strategy to tailor noncollinear magnetic interaction and topological magnetism in the ferromagnet/oxide system.

DOI: [10.1103/PhysRevB.108.214404](https://doi.org/10.1103/PhysRevB.108.214404)

I. INTRODUCTION

The manipulation of interfacial magnetic properties is of great interest in fundamental physics and spintronic applications [1,2]. Dzyaloshinskii-Moriya interaction (DMI) is a kind of antisymmetric magnetic exchange interaction that only exists in systems with spin-orbital coupling (SOC) and inversion symmetry breaking [3]. As a fundamental magnetic ingredient in spin orbitronics, it features in the formation and stabilization of topological magnetism (e.g., magnetic skyrmions and chiral domain walls) as well as the magnetization switching [4]. A strong interfacial DMI (iDMI) can enhance the collapse barriers of skyrmions [5], which is crucial for stabilizing room-temperature skyrmions [6], while the sign of the DMI sets the preferred chirality of the topological magnetism and determines their dynamics properties under current [7]. Hence, how to engineer the DMI has long been of long interest in spintronics.

The iDMI has been induced in many systems, such as ferromagnetic metal/heavy metal (FM/HM) interfaces, Co/graphene [8] (or h -BN [9]) interface, and van der Waals magnet-based heterostructures [10–12]. For the mostly studied magnetic metal films, many methods have been developed to modulate the strength and chirality of iDMI, such as changing the type of substrates [13,14], tuning the thickness of FM [15] and HM [16], applying mechanical strain [17,18],

and controlling the adsorption and desorption of oxygen [19], hydrogen [20,21], and palladium atoms [22] at Ni/Co bilayers. From the point of view of applications, an electrically controlled strategy stands out which is facile and the resulting heat dissipation in this scheme is negligible when comparing with other methods, such as external magnetic field and spin-polarized current [1]. Using electric field to directly control magnetism in metallic films, however, is far more difficult due to the charge-screening length in metal atomic layers being very short and the electric field effect vanishes at only a few atom layers [23]. The voltage-controlled switching of interfacial magnetism properties can be realized in an indirect way, such as through strain-mediated magnetoelastic and magnetoelectric coupling at metallic films [24–26]. For magnetic/oxides interfaces, their built-in electric field renders the voltage direct control of interfacial magnetism possible. Previously, experimental evidence has shown that magnetic anisotropy energy can be effectively modulated by via magnetoionic effects, namely, by controlling the migration of ions (e.g., H^+ and O^{2-}) with voltage via changing interfacial atomic structure and electronic states [19–21]. More recently, this strategy has also been applied to tune the chirality and/or strength of DMI at HM/FM/oxide films [27–31], such as at Ta/CoFeB/TaOx [31] and Pt/Co/MOx trilayers ($M = Al$ or Gd) [29]. However, the existence of heavy elements may cause a large Gilbert damping constant, deteriorating fast chiral magnetization motion at low current density, and even the magnetization switching [3]. Hence, it is interesting to ask if large iDMI and topological magnetism can be realized in a simpler FM/oxide interface without heavy elements, such

*sgwang@ahu.edu.cn

†hongxin.yang@nju.edu.cn

as Fe/MgO, the material prototype in spintronics [32,33]. Previously, most of the studies have focused on the magnetocrystalline anisotropy and magnetoresistance effect of Fe/MgO based nanofilms [33–40]. Recently, the giant Rashba coefficient at 3d FM/MgO interface has been revealed [41], implying that the presence of strong DMI can be possibly induced at the Fe/MgO interface since the strength of the DMI is proportional to the Rashba coefficient [42,43]. The theoretical evidence, however, is still missing [44]. Hence, the interfacial magnetic properties of Fe/MgO have not been fully explored.

Motivated by this issue, we first use first-principles calculations and carefully investigate the Fe/MgO system. We demonstrate that large iDMI that is even comparable to FM/HM bilayer exists in the pure Fe/MgO interface and its chirality is closely related to the thickness of Fe layer. Controlling the interfacial oxidation degree of Fe/MgO bilayers can further engineer the strength and sign of iDMI by tuning the contributions from different Fe-3d orbitals. Next, using micromagnetic simulations, we demonstrate that the significant iDMI gives rise to the formation of chiral spin textures, including magnetic bimerons and skyrmions, at the fully overoxidized Fe(3)/MgO bilayers without applying external magnetic field. These findings prove that the topological magnetism can be achieved in designed 3d FM/oxides interface without heavy metal, which is meaningful toward practical spin-orbitronics devices.

II. COMPUTATIONAL DETAILS

In this paper, all the calculations are performed by using the VASP (Vienna *ab initio* simulation package) [45]. The exchange-correlation energy term is treated with the generalized gradient approximation (GGA) of Perdew-Burke-Ernzerhof (PBE) functionals [46]. The projector augmented-wave approximation (PAW) [47] is adopted to deal with the electron-core interactions. The criterion for energy and force convergences are 1×10^{-7} eV and 0.001 eV/Å, respectively. The plane-wave cutoff energy is set to 520 eV. A vacuum space of more than 15 Å is adopted to reduce the inter-layer interactions due to the periodic boundary conditions. The Monkhorst-Pack k -point mesh of $24 \times 24 \times 1$ is used for sampling 2D Brillouin zone in our self-consistent calculations. To obtain the DMI constant d^{tot} , the chirality-dependent total energy difference approach is adopted [4,48]. A total of $6 \times 24 \times 1$ k -point mesh is employed for a $4 \times 1 \times 1$ supercell to extract DMI parameters. The magnetocrystalline anisotropy (K_{MCA}) energy per unit cell is obtained by calculating the energy difference between the in-plane magnetized [100] axis and the out-of-plane magnetized [001] axis with $E_{\text{MAE}} = E_{100} - E_{001}$, wherein the SOC effect is taken into account. The effective MAE K_{eff} is a sum of the K_{MCA} and dipole-dipole-induced demagnetization energy K_{DD} . K_{DD} is obtained as the difference of the sum of all dipole-dipole interactions up to infinity [37,49], which is calculated by

$$K_{\text{DD}} = E^{\text{dip}}/V_{\text{u.c.}} = -\frac{1}{2} \frac{\mu_0}{4\pi V_{\text{u.c.}}} \times \sum_{i \neq j}^N \frac{1}{r_{ij}^3} \left[\mathbf{M}_i \cdot \mathbf{M}_j - (\mathbf{M}_i \cdot \mathbf{r}_{ij})(\mathbf{M}_j \cdot \mathbf{r}_{ij}) \frac{3}{r_{ij}^2} \right],$$

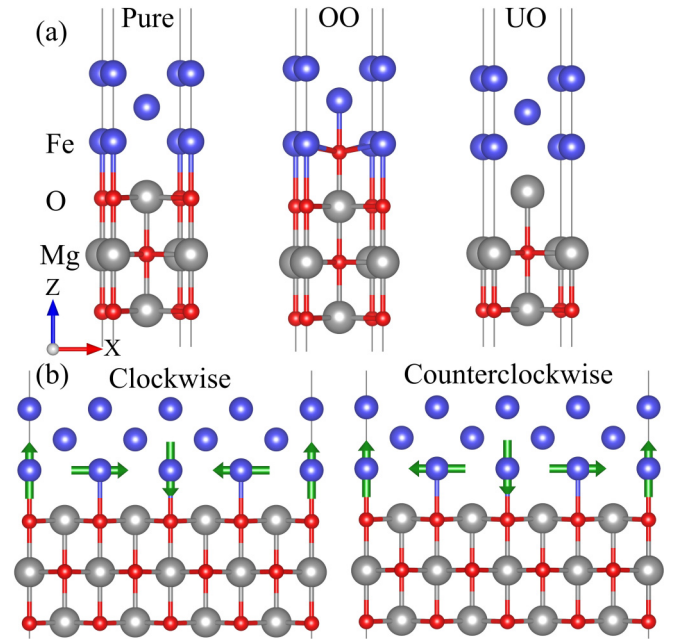


FIG. 1. Schematics of the calculated crystalline structures for (a) pure, overoxidized (OO), and underoxidized (UO) Fe(3)/MgO(3) bilayers. (b) Schematic diagram of Fe(3)/MgO(3) bilayers with clockwise (CW) and counterclockwise (CCW) spin textures, respectively. The arrows indicate spin orientations; Fe, Mg, and O atoms are represented by blue, gray, and red balls, respectively.

in which \mathbf{M}_i and \mathbf{r}_{ij} represent local magnetic moments and a vector connecting site i and j , respectively. A $250 \times 250 \times 1$ supercell is used in K_{DD} calculation to ensure the reliability of results [50]. In our micromagnetic simulations, we use the MUMAX3 package [51] to conduct spin dynamics by solving the Landau-Lifshitz-Gilbert equation,

$$\frac{d\mathbf{M}_i}{dt} = -\gamma \mathbf{M}_i \times \mathbf{H}_i + \frac{\alpha}{M_s} \mathbf{M}_i \times \frac{d\mathbf{M}_i}{dt},$$

where γ is the gyromagnetic ratio, \mathbf{H}_i denotes the effective field of the i th magnetic unit cell \mathbf{M}_i , α represents the Gilbert damping constant ($\alpha = 0.2$ here), and M_s is the saturation magnetization, respectively.

III. STRUCTURES OF PURE, OVEROXIDIZED, AND UNDEROXIDIZED Fe/MgO BILAYERS

To determine the lattice constant of Fe/MgO interface, we fully relax a bulk structure consisting of five Fe and three MgO layers and obtain a lattice constant of 2.966 Å, which is consistent with our previous results [36]. Based on the fixed lattice constant, the optimized pure, fully overoxidized (OO), and fully underoxidized (UO) Fe(3)/MgO(3) interfaces are obtained, as shown in Fig. 1(a). In the following, all the results are calculated with MgO thickness of three layers unless stated otherwise. In Fig. 1(b), we show the schematic diagram of the representative Fe(3)/MgO bilayer with clockwise (CW) (left panel) and counterclockwise (CCW) (right panel) spin chirality in one supercell, respectively. Therein, the same spin chirality configuration is set for all the magnetic

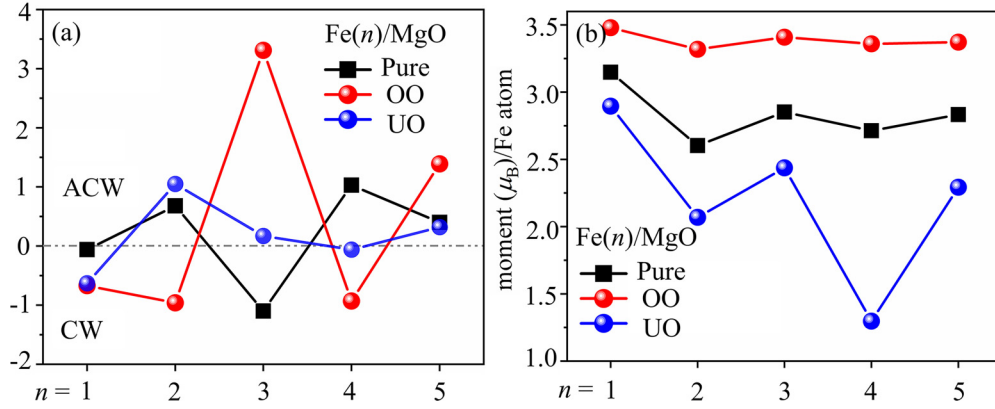


FIG. 2. (a) Calculated DMI strength and (b) magnetic moment of interfacial Fe atom as a function of Fe thickness with different degree of oxidation at Fe/MgO bilayers, respectively.

atomic layers, where only the magnetic moment directions of the Fe layer at the interface are presented as a diagram. After this, the d^{tot} can be obtained via the energy mapping between the CW and CCW chirality by using the formula of $d^{\text{tot}} = (E_{\text{CW}} - E_{\text{CCW}})/8$.

IV. DMI OF THE PURE, OO, AND UO-Fe/MgO BILAYERS

Figure 1(a) shows the calculated total DMI, d^{tot} , of Fe/MgO bilayers with different oxidation degree when the thickness of Fe varies from 1 to 5 monolayers (MLs). For pure or unoxidized interfaces (black cube), one can see that DMI chirality reverses with a period of 1 ML as a function of Fe film thickness (n) up to 4 MLs the chirality remains unchanged when the n is larger than 4. Notably, the d^{tot} of Fe(3)/MgO bilayer is 1.2 meV, which is even comparable to that of the Fe/Ir interface (1.7 meV). Taking account of that there is no heavy elements here, such a magnitude of DMI is sufficiently large but maybe not surprising, because this interface owns strong PMA that is associates with the large

SOC and orbital hybridization, which can also contribute to large DMI. For 100% overoxidized interface (denoted as OO, red balls in Fig. 2), the trends of DMI chirality also reverse with a period of 1 ML as a function of Fe film thickness, but the DMI presents opposite chirality at certain Fe thickness, e.g., Fe(n)/MgO ($n = 2, 3$, and 4), when compared with the pure interface. More importantly, the interfacial oxidation significantly enhances the strength of the DMI, especially at Fe(3)/MgO bilayer, and the d^{tot} is 3.20 meV, which is even larger than the Co/Pt interface. When the interface is totally underoxidized (denoted as UO, blue balls in Fig. 2), the chirality of the DMI can also be changed at certain Fe layers, but the d^{tot} apparently decreases with Fe thickness larger than 3 MLs. These results indicate that both the chirality and strength can be engineered by manipulating interfacial oxygen, e.g., via the field-driven oxygen ionic migration strategy [52–54]. Besides, we notice that the magnitude of the DMI is closely related to the magnetic moment of the interfacial Fe atom. Globally, the d^{tot} at the OO interface is larger than the pure and the UO interfaces at most of the Fe thickness.

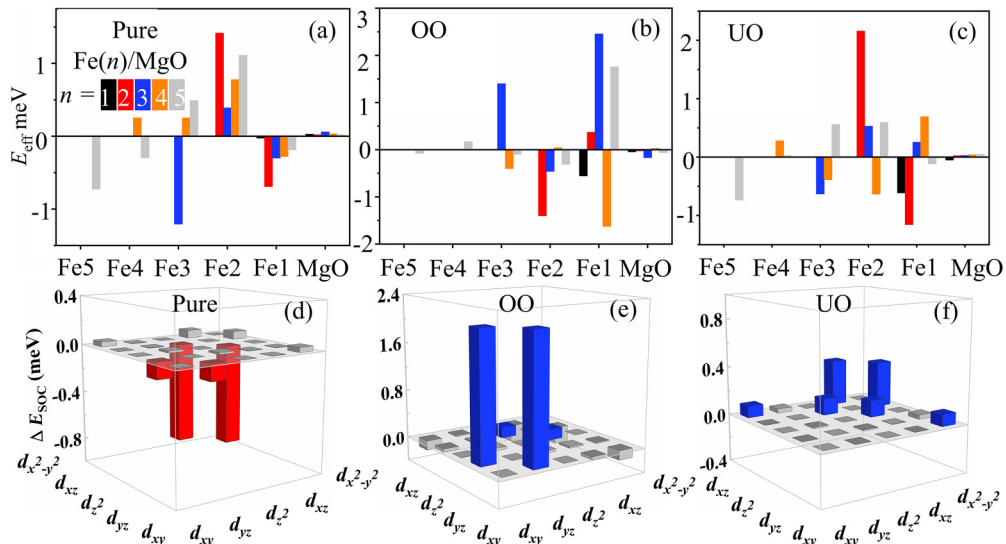


FIG. 3. (a)–(c) Atomic-layer localization of the SOC energy ΔE_{soc} for the different Fe/MgO bilayers; (d), (e) orbital resolved SOC energy matrix elements associated with DMI of Fe in different Fe(3)/MgO(3) bilayers.

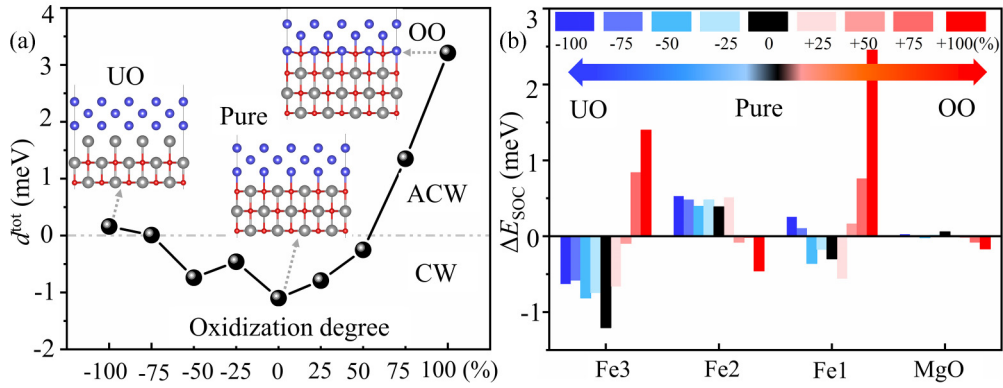


FIG. 4. (a) Calculated DMI strength and (b) atomic-layer-resolved localization of the DMI associated SOC energy ΔE_{soc} as a function of oxidation degree of Fe(3)/MgO(3) bilayers, respectively.

Correspondingly, the moment of the Fe atoms follows the trend of $\mu_B(\text{OO}) > \mu_B(\text{pure}) > \mu_B(\text{UO})$. This means that the DMI strength also follows Hund's rule here, because the DMI is strongly affected by the electronic occupation of the magnetic atom, just similar to the cases of the $3d/5d$ interfaces [13] and Co/hydrogenated graphene interface [55].

V. MICROSCOPIC ORIGIN OF OXIDIZATION ENGINEERED DMI

The microscopic mechanism of DMI at $3d$ FM/oxides (e.g., Co/MgO interface) originates from the Rashba effect [42,56], wherein the interfacial electrostatic potential can compensate for the weak SOC of the nonmagnetic atoms and serve as the effective SOC site to canting the spins. This mechanism is the same as that of the Co/graphene [8] and Co/*h*-BN [9] interfaces but is in stark contrast to the FM/HM interfaces where the DMI stems from the electron scattering of the HM, which can be explained by the Fert-Lévy model [48]. Now, we want to shed further light on the underlying mechanism of how interfacial oxidation changes the DMI. It is clear that the strength of Rashba DMI is associated with the interfacial electric dipole, which can be evaluated by calculating the Rashba coefficients [42]. This method, however, may underestimate the d^{tot} since it only considers the contributions of the splitting band nearest the Fermi surface while the contributions from other bands is not considered, although these bands also play a significant role in determining the total DMI strength [42]. On the other hand, it is clear that the DMI strength is dominated by SOC energy; parsing the atom-resolved ΔE_{soc} to examine the energy source of the DMI is helpful to understand the variations of DMI. According to Figs. 3(a)–3(c), we can see that the change of surface and interfacial Fe atoms dominates the variations of DMI including its sign and strength. For example, for the unoxidized interface [Fig. 3(a)], the ΔE_{soc} of the Fe2 atom in Fe(2)/MgO is positive and is dominant (red bars), giving rise to the CCW chirality of Fe(2)/MgO, while for Fe(3)/MgO (blue bars), the dominant ΔE_{soc} with negative value stems from the surface Fe3 atom, which results in the CW chirality. A similar scenario also happens in the OO- and UO-Fe/MgO bilayers. However, in the UO interfaces [Fig. 3(c)], the ΔE_{soc} energy from different Fe layers present opposite values and cancel each other

thereby lead to the smaller d^{tot} . Notably, the ΔE_{soc} energy of the interfacial and surface Fe atoms at OO-Fe/MgO [Fig. 3(b)] is much stronger than that of the other studied interfaces in most cases, which can explain why the d^{tot} in OO interfaces is the strongest one.

It is clear that the DMI is sensitive to interface electrical states; the change of interface oxygen concentration alters the local structures and inevitably affects the orbital hybridization. We analyze the orbital-resolved SOC contribution to the DMI as shown in Figs. 3(d) and 3(e). Since the d^{tot} peaks in the OO-Fe(3)/MgO and both the sign and strength of DMI experience a dramatic change in the pure-, OO-, and UO-Fe(3)/MgO bilayers, we thus take these three interfaces as a template for further study. Here, we consider the SOC energy matrix elements of $3d$ orbitals of all the Fe atoms, due to the ΔE_{soc} from all the three Fe layers having a non-negligible effect to determine the total DMI strength and sign. One can see that the strongest contribution to DMI comes from the matrix element with d_{xz} and d_z^2 orbitals, which is strongly negative for pure Fe(3)/MgO. However, for the OO-Fe(3)/MgO, the contributions from matrix element of d_{yz} and d_{xy} orbitals predominate with much larger positive values than that of the pure interface, while for the DMI in UO-Fe(3)/MgO, the matrix element of d_{xz} and $d_{x^2-y^2}$ orbitals plays a key role in determining the DMI although these ΔE_{soc} values from these orbitals are quite small. In other words, the interfacial oxidation changes the orbital hybridization between different $3d$ orbitals of Fe atoms and finally defines the sign and magnitude of DMI for Fe/MgO bilayers.

VI. OXIDIZATION DEGREE-DEPENDENT DMI STRENGTH AND CHIRALITY

In a realistic FM/oxides system, the interfaces might be partially oxidized, corresponding to different oxidation degrees, which depends on the diffusion degree of O^{2-} . Since the DMI is sensitive to interfacial atomic structures, its chirality and strength may vary a lot under different oxidation degrees. According to Fig. 4(a), one can see that the DMI of pure Fe(3)/MgO(3) bilayer is -1.20 meV/atom and presents CW chirality. As we reduce the oxidation degree from the pure interface to a fully UO state (-100%), the strength of DMI sharply decreases and the sign of DMI is also varied to

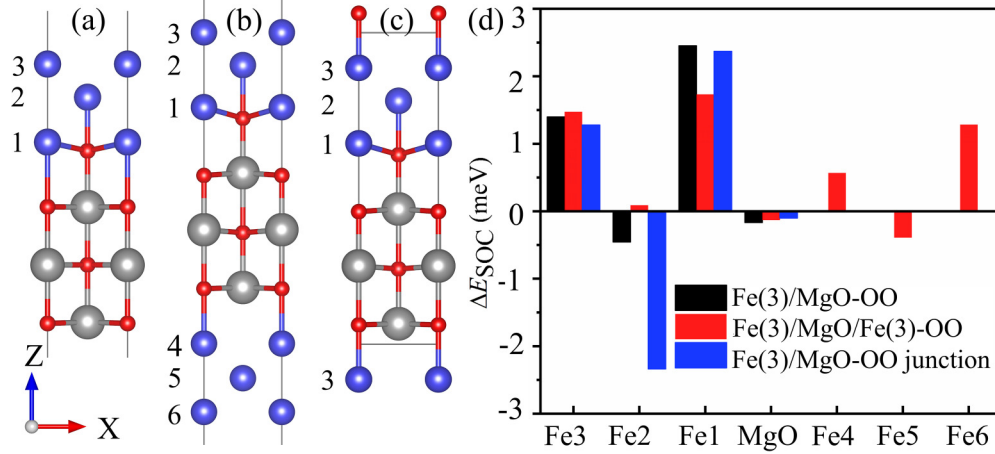


FIG. 5. (a) Schematics of the crystalline structures for (a) Fe(3)/MgO-OO bilayer, Fe(3)/MgO/Fe(3)-OO trilayer, and Fe(3)/MgO-OO junction, respectively. (b) The corresponding atomic-layer-resolved localization of the DMI associated SOC energy ΔE_{soc} for the aforementioned Fe/MgO systems, respectively.

CCW. While enhancing the oxidization degree from 0 to 50%, the strength of DMI decreases but with identical chirality; further enhancing the oxidization degree to 100% will significantly increase the magnitude of DMI and inverse its chirality from CW to CCW. These results indicate that both the strength and chirality of DMI are sensitive to the interfacial structure of Fe/MgO bilayer and can be engineered by manipulating the interfacial oxidization degree, e.g., gate-controlled O^{2-} migration.

To further understand the underlying mechanism, we carefully analyze the atomic-layer-resolved localization of the DMI associated SOC energy ΔE_{soc} of the representative Fe(3)/MgO bilayers with different oxidization degrees, which is shown in Fig. 4(b). One can see that the ΔE_{soc} contributions from the Fe atoms (Fe1) at the OO-Fe/MgO interface (red bar) sharply increase with gradually improving the oxidization degree. Since the dominated ΔE_{soc} energy at the surface Fe3 and middle Fe2 atom layers presents opposite values, they cancel each other out and thus decrease the total DMI strength as the interfacial oxygen concentration gradually decreases (blue bars of UO). In addition, we notice that for all the scenarios the ΔE_{soc} of the Fe atoms at the surface contributes

a lot to the total DMI, indicating the importance of surface effect of Fe/MgO bilayers. The possible reason behind this is that the inversion symmetry breaking at the metal surface (or metal/vacuum interface) renders electric field couples to the spin of itinerant electrons and causes the Rashba effect [57], giving rise to the large SOC contributions to the total DMI. Such a kind of surface effect induced Rashba SOC has also been reported in some conventional metals (such as Au and Bi) [58] and topological insulators [59].

VII. DMI AT OO-FE/MGO SYSTEM

The aforementioned results inspire us to investigate whether novel physical properties can exist in a designed Fe/MgO system. Here, we choose the 100% OO-Fe(3)/MgO bilayer as the basic prototype to further design the system, due to its giant DMI. In the metallic heterostructures, it is known that the DMI in Fe/Ir is CCW chirality and is CW chirality in Pt/Co bilayer [48]. Constructing a Pt/Co/Fe/Ir multilayer can further enhance the total DMI strength [6], which is crucial for realizing room-temperature magnetic skyrmions. According to our calculation, the DMI chirality of pure and

TABLE I. The calculated film thickness t , saturation magnetization M_s , DMI parameter D , and effective MAE K_u .

Structures	t (Å)	M_s ($\mu_B/\text{f.u.}$)	K_u (mJ/m ³)	D (mJ/m ²)
Fe/MgO-Pure Fe(1)/MgO	2.15	3.18	9.91	-0.22
Fe(2)/MgO	3.20	5.46	1.25	1.24
Fe(3)/MgO	4.73	8.31	4.81	-1.34
Fe/MgO-OO Fe(1)/MgO	2.20	3.76	-8.36	-2.29
Fe(2)/MgO	5.02	6.76	-3.63	-1.82
Fe(3)/MgO	5.30	9.23	-2.96	3.89
Fe/MgO-UO Fe(1)/MgO	1.70	1.64	-4.29	-2.40
Fe(2)/MgO	2.82	4.80	3.42	1.89
Fe(3)/MgO	4.29	7.81	1.10	0.19
Fe(3)/MgO/Fe(3)-OO	8.50	17.52	2.17	2.80
MgO/Fe(3)-OO junction	5.40	9.37	-1.85	1.60

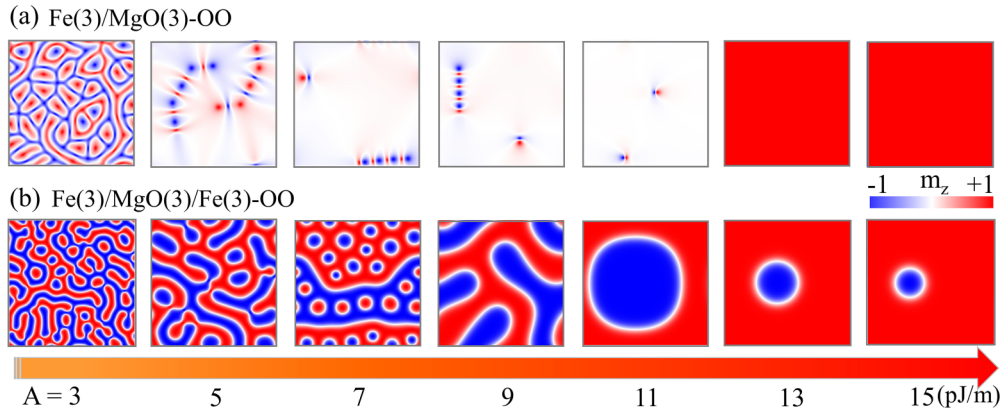


FIG. 6. (a) Relaxed spin configurations of (a) Fe(3)/MgO(3)-OO bilayer and (b) Fe(3)/MgO(3)/Fe(3)-OO trilayer as a function of exchange stiffness A that is in the range 3–15 pJ/m, respectively. We use $120 \times 120 \text{ nm}^2$ square with the periodic boundaries in the micromagnetic simulation process. The color map indicates the out-of-plane spin component of Fe atoms.

OO-Fe(3)/MgO is CW and CCW, respectively. Once the two interfaces are combined and form Fe(3)/MgO/Fe(3)-OO trilayer, we find that the magnitude of DMI is largely enhanced to 4.21 meV, since the ΔE_{soc} of the Fe atoms at all interfaces contributes to the total DMI strength positively [red bars in Fig. 5(a)], while the d^{tot} (1.32 meV) in the oxidized Fe/MgO/Fe junction is not as large as the Fe(3)/MgO/Fe(3)-OO trilayer, due to the dominating ΔE_{soc} from the interfacial Fe1 and middle Fe2 being of the opposite sign [blue bars in Fig. 5(b)].

VIII. TOPOLOGICAL MAGNETISM AT THE DESIGNED Fe/MgO FILMS

We use MUMAX3 code to test whether topological magnetism can be realized in the designed Fe/MgO system. Therein, the DMI and MAE have been obtained from our first-principles calculations, but the magnetic parameter of exchange stiffness constant A is hard to evaluate theoretically due to the itinerant magnetic nature of the system [60]. To access this dilemma, we use the A in a large range of 3–15 pJ/m, which is less than that of the bulk fcc Fe metal ($\sim 19 \text{ pJ/m}$) [61]. With all the determined magnetic parameters of the Fe/MgO system (see Table I), we can now perform micromagnetic simulations with $120 \text{ nm} \times 120 \text{ nm}$ scale from an initial random magnetic state (see Fig. 6). After the relaxation, a bimeron state emerges in the OO-Fe(3)/MgO bilayer when A is smaller than 13 pJ/m, while the skyrmion state can be realized in Fe(3)/MgO/Fe(3)-OO trilayer in all the range of A . Such a difference of topological magnetism originates from the K_u , since the in-plane (out-of-plane) magnetic orientation of the bilayer (trilayer) favors the formation of bimeron and skyrmion states, respectively. These results demonstrate that the chiral spin texture can be possibly stabilized in the

designed Fe/MgO system, which is useful for topological spintronic devices.

IX. CONCLUSION

In summary, we verify the presence of significant non-collinear magnetic interaction (DMI) at the Fe/MgO interface. More specially, both the chirality and strength of DMI can be engineered by manipulating the oxidization degree of the interface due to the oxidization induced orbital reconstruction of Fe-3d. In addition, we predict that different chiral spin textures can be achieved in the designed Fe/MgO films, indicating the exotic magnetic phenomenon in the prototype material in spintronics. These results not only enrich the physics of the Fe/MgO system but also it is meaningful to tailor the DMI and topological magnetism at other FM/oxide interfaces though an electrically controlled ionic migration strategy.

ACKNOWLEDGMENTS

We thank Prof. H. Huang from the University of Science and Technology Beijing for the discussion. This work was supported by the National Key Research and Development Program of China (MOST) (Grant No. 2022YFA1405102), the National Natural Science Foundation of China (Grants No. 12174405, No. 52130103, and No. 51971026), Ningbo Key Scientific and Technological Project (Grant No. 2021000215), “Pioneer” and “Leading Goose” R&D Program of Zhejiang Province (Grant No. 2022C01053), Beijing National Laboratory for Condensed Matter Physics (Grant No. 2021000123), and China Postdoctoral Science Foundation (Grants No. 2021M703314 and No. 2022T150669).

- [1] F. Matsukura, Y. Tokura, and H. Ohno, *Nat. Nanotechnol.* **10**, 209 (2015).
 [2] F. Hellman, A. Hoffmann, Y. Tserkovnyak, G. S. D. Beach, E. E. Fullerton, C. Leighton, A. H. MacDonald, D. C. Ralph,

- D. A. Arena, H. A. Dürr, P. Fischer, J. Grollier, J. P. Heremans, T. Jungwirth, A. V. Kimel, B. Koopmans, I. N. Krivorotov, S. J. May, A. K. Petford-Long, J. M. Rondinelli *et al.*, *Rev. Mod. Phys.* **89**, 025006 (2017).

- [3] A. Fert, N. Reyren, and V. Cros, *Nat. Rev. Mater.* **2**, 17031 (2017).
- [4] H. Yang, J. Liang, and Q. Cui, *Nat. Rev. Phys.* **5**, 43 (2023).
- [5] F. Muckel, S. von Malottki, C. Holl, B. Pestka, M. Pratzner, P. F. Bessarab, S. Heinze, and M. Morgenstern, *Nat. Phys.* **17**, 395 (2021).
- [6] A. Soumyanarayanan, M. Raju, A. L. Gonzalez Oyarce, A. K. C. Tan, M.-Y. Im, A. P. Petrović, P. Ho, K. H. Khoo, M. Tran, C. K. Gan, F. Ernult, and C. Panagopoulos, *Nat. Mater.* **16**, 898 (2017).
- [7] S. Emori, U. Bauer, S.-M. Ahn, E. Martinez, and G. S. D. Beach, *Nat. Mater.* **12**, 611 (2013).
- [8] H. Yang, G. Chen, A. A. C. Cotta, A. T. N'Diaye, S. A. Nikolaev, E. A. Soares, W. A. A. Macedo, K. Liu, A. K. Schmid, A. Fert, and M. Chshiev, *Nat. Mater.* **17**, 605 (2018).
- [9] A. Hallal, J. Liang, F. Ibrahim, H. Yang, A. Fert, and M. Chshiev, *Nano Lett.* **21**, 7138 (2021).
- [10] Y. Wu, S. Zhang, J. Zhang, W. Wang, Y. L. Zhu, J. Hu, G. Yin, K. Wong, C. Fang, C. Wan, X. Han, Q. Shao, T. Taniguchi, K. Watanabe, J. Zang, Z. Mao, X. Zhang, and K. L. Wang, *Nat. Commun.* **11**, 3860 (2020).
- [11] T.-E. Park, L. Peng, J. Liang, A. Hallal, F. S. Yasin, X. Zhang, K. M. Song, S. J. Kim, K. Kim, M. Weigand, G. Schütz, S. Finizio, J. Raabe, K. Garcia, J. Xia, Y. Zhou, M. Ezawa, X. Liu, J. Chang, H. C. Koo *et al.*, *Phys. Rev. B* **103**, 104410 (2021).
- [12] D. Li, S. Haldar, and S. Heinze, *Nano Lett.* **22**, 7706 (2022).
- [13] A. Belabbes, G. Bihlmayer, F. Bechstedt, S. Blügel, and A. Manchon, *Phys. Rev. Lett.* **117**, 247202 (2016).
- [14] X. Ma, G. Yu, C. Tang, X. Li, C. He, J. Shi, K. L. Wang, and X. Li, *Phys. Rev. Lett.* **120**, 157204 (2018).
- [15] J. Cho, N.-H. Kim, S. Lee, J.-S. Kim, R. Lavrijsen, A. Solignac, Y. Yin, D.-S. Han, N. J. J. van Hoof, H. J. M. Swagten, B. Koopmans, and C.-Y. You, *Nat. Commun.* **6**, 7635 (2015).
- [16] S. Tacchi, R. E. Troncoso, M. Ahlberg, G. Gubbiotti, M. Madami, J. Akerman, and P. Landeros, *Phys. Rev. Lett.* **118**, 147201 (2017).
- [17] N. S. Gusev, A. V. Sadovnikov, S. A. Nikitov, M. V. Sapozhnikov, and O. G. Udalov, *Phys. Rev. Lett.* **124**, 157202 (2020).
- [18] C. Feng, F. Meng, Y. Wang, J. Jiang, N. Mehmood, Y. Cao, X. Lv, F. Yang, L. Wang, Y. Zhao, S. Xie, Z. Hou, W. Mi, Y. Peng, K. Wang, X. Gao, G. Yu, and J. Liu, *Adv. Funct. Mater.* **31**, 2008715 (2021).
- [19] G. Chen, A. Mascaraque, H. Jia, B. Zimmermann, M. Robertson, R. L. Conte, M. Hoffmann, M. A. G. Barrio, H. Ding, R. Wiesendanger, E. G. Michel, S. Blügel, A. K. Schmid, and K. Liu, *Sci. Adv.* **6**, eaba4924 (2020).
- [20] G. Chen, M. C. Robertson, M. Hoffmann, C. Ophus, A. L. Fernandes Cauduro, R. Lo Conte, H. Ding, R. Wiesendanger, S. Blügel, A. K. Schmid, and K. Liu, *Phys. Rev. X* **11**, 021015 (2021).
- [21] G. Chen, C. Ophus, A. Quintana, H. Kwon, C. Won, H. Ding, Y. Wu, A. K. Schmid, and K. Liu, *Nat. Commun.* **13**, 1350 (2022).
- [22] G. Chen, C. Ophus, R. Lo Conte, R. Wiesendanger, G. Yin, A. K. Schmid, and K. Liu, *Nano Lett.* **22**, 6678 (2022).
- [23] T. Srivastava, M. Schott, R. Juge, V. Křížáková, M. Belmeguenai, Y. Roussigné, A. Bernand-Mantel, L. Ranno, S. Pizzini, S.-M. Chérif, A. Stashkevich, S. Auffret, O. Boulle, G. Gaudin, M. Chshiev, C. Baraduc, and H. Béa, *Nano Lett.* **18**, 4871 (2018).
- [24] J.-M. Hu, T. Yang, and L.-Q. Chen, *Npj Comput. Mater.* **4**, 62 (2018).
- [25] Y. Wang, L. Wang, J. Xia, Z. Lai, G. Tian, X. Zhang, Z. Hou, X. Gao, W. Mi, C. Feng, M. Zeng, G. Zhou, G. Yu, G. Wu, Y. Zhou, W. Wang, X.-x. Zhang, and J. Liu, *Nat. Commun.* **11**, 3577 (2020).
- [26] Y. Ba, S. Zhuang, Y. Zhang, Y. Wang, Y. Gao, H. Zhou, M. Chen, W. Sun, Q. Liu, G. Chai, J. Ma, Y. Zhang, H. Tian, H. Du, W. Jiang, C. Nan, J.-M. Hu, and Y. Zhao, *Nat. Commun.* **12**, 322 (2021).
- [27] R. Mishra, D. Kumar, and H. Yang, *Phys. Rev. Appl.* **11**, 054065 (2019).
- [28] L. Herrera Diez, Y. T. Liu, D. A. Gilbert, M. Belmeguenai, J. Vogel, S. Pizzini, E. Martinez, A. Lamperti, J. B. Mohammedi, A. Laborieux, Y. Roussigné, A. J. Grutter, E. Arenholtz, P. Quarterman, B. Maranville, S. Ono, M. S. E. Hadri, R. Tolley, E. E. Fullerton, L. Sanchez-Tejerina *et al.*, *Phys. Rev. Appl.* **12**, 034005 (2019).
- [29] D. de S. Chaves, F. Ajejas, V. Křížáková, J. Vogel, and S. Pizzini, *Phys. Rev. B* **99**, 144404 (2019).
- [30] M. Arora, J. M. Shaw, and H. T. Nembach, *Phys. Rev. B* **101**, 054421 (2020).
- [31] C.-E. Fillion, J. Fischer, R. Kumar, A. Fassatoui, S. Pizzini, L. Ranno, D. Ourdani, M. Belmeguenai, Y. Roussigné, S.-M. Chérif, S. Auffret, I. Joumard, O. Boulle, G. Gaudin, L. Buda-Prejbeanu, C. Baraduc, and H. Béa, *Nat. Commun.* **13**, 5257 (2022).
- [32] W. H. Butler, X. G. Zhang, T. C. Schulthess, and J. M. MacLaren, *Phys. Rev. B* **63**, 054416 (2001).
- [33] S. Yuasa, T. Nagahama, A. Fukushima, Y. Suzuki, and K. Ando, *Nat. Mater.* **3**, 868 (2004).
- [34] Q.-f. Zhan, S. Vandezande, K. Temst, and C. Van Haesendonck, *New J. Phys.* **11**, 063003 (2009).
- [35] T. Maruyama, Y. Shiota, T. Nozaki, K. Ohta, N. Toda, M. Mizuguchi, A. A. Tulapurkar, T. Shinjo, M. Shiraishi, S. Mizukami, Y. Ando, and Y. Suzuki, *Nat. Nanotechnol.* **4**, 158 (2009).
- [36] H. X. Yang, M. Chshiev, B. Dieny, J. H. Lee, A. Manchon, and K. H. Shin, *Phys. Rev. B* **84**, 054401 (2011).
- [37] A. Hallal, H. X. Yang, B. Dieny, and M. Chshiev, *Phys. Rev. B* **88**, 184423 (2013).
- [38] F. Ibrahim, H. X. Yang, A. Hallal, B. Dieny, and M. Chshiev, *Phys. Rev. B* **93**, 014429 (2016).
- [39] J. W. Koo, S. Mitani, T. T. Sasaki, H. Sukegawa, Z. C. Wen, T. Ohkubo, T. Niizeki, K. Inomata, and K. Hono, *Appl. Phys. Lett.* **103**, 192401 (2013).
- [40] S. G. Wang, R. C. C. Ward, G. X. Du, X. F. Han, C. Wang, and A. Kohn, *Phys. Rev. B* **78**, 180411(R) (2008).
- [41] O. Rousseau, C. Gorini, F. Ibrahim, J.-Y. Chauleau, A. Solignac, A. Hallal, S. Tölle, M. Chshiev, and M. Viret, *Phys. Rev. B* **104**, 134438 (2021).
- [42] H. Yang, O. Boulle, V. Cros, A. Fert, and M. Chshiev, *Sci. Rep.* **8**, 12356 (2018).
- [43] J. Liang, Q. Cui, and H. Yang, *Phys. Rev. B* **102**, 220409(R) (2020).
- [44] K. Nawaoka, S. Miwa, Y. Shiota, N. Mizuochi, and Y. Suzuki, *Appl. Phys. Express* **8**, 063004 (2015).
- [45] G. Kresse and J. Furthmüller, *Phys. Rev. B* **54**, 11169 (1996).

- [46] J. P. Perdew, K. Burke, and M. Ernzerhof, *Phys. Rev. Lett.* **77**, 3865 (1996).
- [47] G. Kresse and D. Joubert, *Phys. Rev. B* **59**, 1758 (1999).
- [48] H. Yang, A. Thiaville, S. Rohart, A. Fert, and M. Chshiev, *Phys. Rev. Lett.* **115**, 267210 (2015).
- [49] G. H. O. Daalderop, P. J. Kelly, and M. F. H. Schuurmans, *Phys. Rev. B* **41**, 11919 (1990).
- [50] L. Vojáček, F. Ibrahim, A. Hallal, B. Dieny, and M. Chshiev, *Phys. Rev. Appl.* **15**, 024017 (2021).
- [51] A. Vansteenkiste, J. Leliaert, M. Dvornik, M. Helsen, F. Garcia-Sanchez, and B. V. Waeyenberge, *AIP Adv.* **4**, 107133 (2014).
- [52] C. Bi, Y. Liu, T. Newhouse-Illige, M. Xu, M. Rosales, J. W. Freeland, O. Mryasov, S. Zhang, S. G. E. te Velthuis, and W. G. Wang, *Phys. Rev. Lett.* **113**, 267202 (2014).
- [53] U. Bauer, L. Yao, A. J. Tan, P. Agrawal, S. Emori, H. L. Tuller, S. van Dijken, and G. S. D. Beach, *Nat. Mater.* **14**, 174 (2015).
- [54] C. Leighton, *Nat. Mater.* **18**, 13 (2019).
- [55] B. Yang, Q. Cui, J. Liang, M. Chshiev, and H. Yang, *Phys. Rev. B* **101**, 014406 (2020).
- [56] O. Boulle, J. Vogel, H. Yang, S. Pizzini, D. de Souza Chaves, A. Locatelli, T. O. Mentes, A. Sala, L. D. Buda-Prejbeanu, O. Klein, M. Belmeguenai, Y. Roussigné, A. Stashkevich, S. M. Chérif, L. Aballe, M. Foerster, M. Chshiev, S. Auffret, I. M. Miron, and G. Gaudin, *Nat. Nanotechnol.* **11**, 449 (2016).
- [57] A. Soumyanarayanan, N. Reyren, A. Fert, and C. Panagopoulos, *Nature (London)* **539**, 509 (2016).
- [58] A. Manchon, H. C. Koo, J. Nitta, S. M. Frolov, and R. A. Duine, *Nat. Mater.* **14**, 871 (2015).
- [59] M. Z. Hasan and C. L. Kane, *Rev. Mod. Phys.* **82**, 3045 (2010).
- [60] B. Zimmermann, G. Bihlmayer, M. Böttcher, M. Bouhassoune, S. Lounis, J. Sinova, S. Heinze, S. Blügel, and B. Dupé, *Phys. Rev. B* **99**, 214426 (2019).
- [61] C. A. F. Vaz, J. A. C. Bland, and G. Lauhoff, *Rep. Prog. Phys.* **71**, 056501 (2008).